# Numerical Simulations of Sintering Coupled with Moisture Transfer

P. Rando, J. Engmann, B. Watzke, L. Forny, V. Meunier, M. Ramaioli

# Numerical Simulations of Sintering Coupled with Moisture Transfer

P. Rando[a], J. Engmann[b], B. Watzke[c], L. Forny[d], V. Meunier[b], M. Ramaioli[a]

[a] *UMR SayFood, Université Paris-Saclay, AgroParisTech, INRAE, 78850, Thiverval Grignon, France*

[b] *Societé des Produits Nestlé S.A., Nestlé Research, PO Box 44, 1000 Lausanne 26, Switzerland*

[c] *Societé des Produits Nestlé S.A., Nestlé Research, PO Box 44, 1000 Lausanne 26, Switzerland. Current address : CH-1012, Lausanne, Switzerland*

[d] *Société des Produits Nestlé SA, Nestlé Research and Development, Orbe, Switzerland*

---

**Abstract**

In many applications, amorphous particles bond together through a phenomenon known as sintering to minimize their surface energy. Water is a plasticizer for many food and pharmaceutical powders and the strong reduction in viscosity induced by moisture absorption can accelerate strongly particle sintering [1]. Numerical simulations of particle sintering usually neglect the coupling with moisture transfer, considering a uniform viscosity throughout the particle.

In this study, a novel approach based on solving Navier-Stokes equation using an Arbitrary Lagrangian–Eulerian (ALE) approach is proposed to model the dynamics of particle sintering coupled with moisture transfer. Maltodextrin DE21 is considered as an industrially relevant example of amorphous particles. Due to moisture uptake, strong gradients of viscosity can exist in the particles undergoing sintering.

FEM simulations consider accurately the forces acting on the contact

area between the particles, leading to slower dynamics than commonly used approximate analytical models. This study highlights that FEM simulations considering a homogeneous moisture and viscosity within the particles are in many cases sufficiently accurate and identifies the limits of validity of this assumption. In the conditions considered in this study, the intraparticle gradients were found to condition significantly the sintering dynamics only when particle diameter is above 1.5mm. The particle size affects strongly both the dynamics of sintering and of moisture transfer. Moreover, higher external relative humidity leads to a lower viscosity and a faster sintering kinetics. The initial water content was found to have a lower impact in the conditions studied.

This coupled simulation approach can be used to identify conditions reducing the risk of caking during the storage of amorphous powders or to master sintering during powder structuration processes. Furthermore this study helps identifying when simpler simulation approaches considering homogeneous particles can be safely used and shows the limitations of simplified analytical models.

*Keywords:* Sintering, Interfacial Flows, Moisture Transfer, Amorphous Polysaccarides

---

## 1. Introduction

Bulk materials, during handling, processing or storage are often exposed to fluctuating environmental conditions. Higher external relative humidity and temperature can induce moisture and heat transfer, changing the material physical properties. In amorphous powders, when the local temperature

exceeds the glass transition temperature, viscous flow takes place between adjacent particles [2]. An undesired phenomenon, known as caking, can occur leading to the agglomeration of several particles which sinter together. This phenomenon may also be induced by the absorption of water that lowers the glass transition temperature below the storage temperature [1].

The Brunauer– Emmett–Teller (BET) or the Guggenheim-Anderson-de Boer (GAB) model ([1], [3]) are commonly used in the literature to model the sorption isotherm behaviours of food amorphous polysaccharides. Lowering of the glass transition temperature and viscosity are frequently modeled with a Gordon-Taylor and Williams-Landel-Ferry model, respectively. Recently, Ubbink *et al.* [4] proposed a modified WLF equation where the constant $C_2$ depends on the water content following a Gordon-Taylor- like behaviour. Experimental data of amorphous food systems showed good agreement in a range of viscosity between 10 and $10^8 Pa \cdot s$.

Sintering occurs between two adjacent particles, when they tend to bond together driven by the surface tension and slowed down by viscous dissipation. The overall sintering process may be described in four steps: at the beginning the surface of two particles with an initial amount of water are placed in contact; secondly a small bridge forms between the two particles, during this step the temperature needs to be higher than $T_g$; thirdly the neck formed between the two particles grows. Finally, to minimize their surface energy the particles fully coalesce, forming a single final particle with a bigger diameter. The sintering dynamics are mainly influenced by materials surface tension and viscosity and the size and shape of the particles [2]. In particular, a higher viscosity and particle size results in slowing down

the bridge growth, due to a higher resistance to the flow; whereas a higher surface tension enhances the sintering kinetics.

The sintering behaviour has been investigated in the literature for different types of materials such as plastic polymers, ceramic and also amorphous food materials, through semi-empirical and numerical models. In general authors refer to particles having a regular shapes, such as spheres or cylinders and consider a Newtonian behaviour to simplify the problem. Frenkel [5] and Pokluda [6] studied the coalescence of two Newtonian spherical particles. The Frenkel-Eshelby model assumes a constant radius and it is valid only for the first stages of sintering. On the contrary, the Pokluda model is based on the balance between the surface tension work and the viscous dissipation and can be used to predict the overall sintering kinetic, neglecting the effect of the gravity. Hopper [7] solved analytically a model to predict the full coalescence of two cylinders, under the assumption of infinite length. Rumpf *et al.* [1] proposed a model to predict the sintering of Newtonian spherical particles based on the Navier-Stokes equation and considering an external force pressing the particles together.

Simple experiments were carried out placing in contact two particle in a controlled temperature and RH environment while the bridge was measured over time using an optical microscope. Bellehumeur *et al.* [8] studied the sintering of different type of polyethylene particles and found good agreement with the Hopper model; whereas the Frenkel's model is not able to describe these experimental data. Hartmann and Descamps ([1], [9]) measured experimentally the sintering between two maltodextrin particles and correlated the measured bridge size to the strength of the caked powders, considering a

Rumpf model with an effective viscosity.

Numerical simulation has been used to study the sintering of spherical particles having a constant viscosity ([10], [11], [12], [13]). This approach can be addressed using different methods such as Lagrangian-Eulerian (ALE) or Eulerian-Eulerian [14]. In the ALE methods, the domain grid moves according to the geometric constrains, typically the motion of the free surface. The grid deforms over time while particles sintering is driven by the surface tension applied on the free surface boundaries. The mesh quality decreases over time decreasing the accuracy therefore a periodic remeshing is often needed [14]. On the other hand, level set methods follow an Eulerian-Eulerian approach where the conservation of mass, momentum and energy balances are solved considering the volume fraction and the material properties of each phase [15]. This method is suitable to model sharp interfaces; however since all the immiscible phases are modelled it is computationally more expensive.

Non-isothermal sintering of polymeric plastic particles has been studied by Kamyabi *et al.* [16]. Firstly, a dimensionless number was defined to compare the characteristic timescales of heat transfer and sintering. The authors highlight the importance of coupling the heat transfer and sintering whenever the timescales have the same order of magnitude. The Kamyabi number was estimated considering an average effective viscosity, that could lead to under or overestimation. In fact, the presence of strong viscosity gradients into particles can still affect the viscosity dynamics. Secondly, Kamyabi coupled the Pokluda and Frenkel-Eshelby models with a thermal dependency of the viscosity. In particular, the viscosity dependency has been described considering linear, exponential and WLF models. A similar

approach has been used by Hartmann *et al.* [1] who investigated the sintering kinetics of maltodextrin DE21 particles, relating the average viscosity to the glass transition temperature and the water content. In both these studies, an average effective viscosity was considered to predict the bridge growth between particles. However, heat and mass transfer can cause strong viscosity gradient into the particles, affecting the sintering dynamics.

Models in the literature are able to predict the sintering dynamics of particles with a homogeneous composition and viscosity distributions. However, whenever strong gradients in the water content exist and the viscosity has a strong dependence on the water content the sintering dynamics is more complex and numerical simulations coupling the sintering with moisture transfer need to be considered.

Based on these premises, in this article we propose a computational model to predict the sintering dynamics of two spherical particles coupled to the moisture transfer. A change of relative humidity leads to moisture transfer into the particles and affects the sintering dynamics due to the strong dependence of the viscosity from the water content. BET, Gordon-Taylor and WLF models are used respectively to model the sorption isotherm, glass transition temperature and viscosity. In this study, we have considered that vapour condensation and dissolution are slow compared to the other phenomena, there are situation where this may not be valid. MD DE-21 was used as a model material, however the model can be extended to predict the sintering of amorphous polymers, whenever strong viscosity gradients exist.

## 2. Materials & Methods

In this section, we firstly present the main dimensionless numbers derived from dimension analysis and the assumptions considered for the derivation of the sintering model. Secondly, the computational model used to investigate the sintering coupled to moisture transfer between two spherical particles will be presented.

### *2.1. Dimension Analysis*

Maltodextrin DE-21 was chosen as model material. Its physical properties are reported in tables A.1 and A.2. Since larger particle size slows down both the sintering and mass transfer dynamics, a diameter of 300 $\mu m$ was considered during preliminary calculations.

Reynolds number expresses the ratio between inertia and viscous forces. The initial diameter ($d_0$) of the particle was considered as characteristic length; whereas the velocity was assumed equal to $v \approx \gamma/\eta_0$, as proposed by Van de Vorst *et al.* [13].

$$Re = \frac{\rho v d_0}{\eta_0} \approx 2.27 \cdot 10^{-14} \tag{1}$$

The order of magnitude of $Re$ shows that maltodextrin flows in the creeping flow regime. Moreover, the Eotvos number was considered to evaluate the ratio between the gravitational and capillary forces.

$$Eo = \frac{\rho g d_0^2}{\gamma} = 0.02 \tag{2}$$

Eo was found to be smaller than 0.1, meaning that the gravitational forces are negligible for particles having a diameter smaller then 300 $\mu m$.

The mass transfer coefficient $K$ between air and maltodextrin was estimated considering a Sherwood number for spherical particles, where the characteristic length was assumed to be equal to the initial diameter ($d_0$) and the diffusivity of air ($D_{air}$) was taken at room temperature.

$$Sh = \frac{K \cdot L}{D_{air}} = 2; \quad D_{air} = 0.219 \quad [cm^2/s]; \quad and \quad L = d_0 \tag{3}$$

Kamyabi *et al.* [16] proposed a dimensionless number to compare the timescales of heat transfer and sintering between two particles. In this study, we defined a Kamyabi number to compare the timescales between moisture transfer and sintering. The characteristic timescales of mass transfer has been computed considering the diffusion into the particles as limiting step. Moreover, accordingly to Kamyabi *et al.* [16] calculation were made considering an average viscosity $\bar{\eta}$ and $d_0 = [300, 1500]\mu m$ to emphasis the effect of the particle size on the viscosity gradients.

$$N_{m,s} = \frac{t_m}{t_s} = \frac{\frac{d_0^2}{4D_{H_2O-MD}}}{\frac{\bar{\eta} d_0}{2\gamma}} = \frac{d_0 \gamma}{2\bar{\eta} D_{H_2O-MD}} = [0.052 - 0.262] \tag{4}$$

The value of $N_{m,s}$ shown above suggests that characteristic sintering time is higher respect to the moisture transfer; however, when particles are sufficiently large, $t_s$ and $t_m$ are similar, and the evolution in time of the mass transfer has an impact on the sintering dynamics.

Finally, the Biot number compares diffusion within a body and mass convection to its surface and can be used to judge on whether the water concentration is uniform within the body. It can be expressed as:

$$Bi = \frac{K d_0}{D_{H_2O-MD}} = [0.015 - 4.38] \cdot 10^8 \quad (5)$$

The range computed for this application suggest that the diffusion within the particle is much slower than the mass transfer at the surface, thus inducing gradients in water content. Moreover, since the viscosity depends strongly on the concentration, even small changes in the concentration can lead to high viscosity gradients during sintering.

### *2.2. Sintering Model Coupled with Moisture Transfer*

Figure A.1 shows schematically the different stages which occur during the sintering of two particles of maltodextrin, while the moisture transfers into the particles. At the initial time ($t = 0$) particles are in contact and contain a certain amount of water due to the initial environmental relative humidity ($RH_0$). Afterwards, an initial bridge between the two particles forms. The particle bridge grows driven by the surface tension, after the RH is increased and the amount of water begins to increase. This causes a drastic decrease of the local viscosity which enhances the sintering kinetics. Finally, particles form a single final spherical particle with a higher final diameter ($d_f = 1.26 \cdot d_0$) [6].

The 3D geometry of the two particles has been simplified considering 2D axial-symmetry along the z-axis and a symmetrical boundary condition along the r-axis (Fig. A.1), allowing to significantly decrease the computational costs of the simulations. Moreover, a small initial bridge, $x_0$, has been set between the two particles to avoid singularity. The effect of the initial bridge is discussed in Appendix A.1.

After the contact occurs the two particles flow following a Navier-Stokes equation (Eq. 6):

$$\rho(\frac{\partial \mathbf{u}}{\partial t} + \mathbf{u} \cdot \nabla \mathbf{u}) - \nabla \cdot (\eta(\nabla \mathbf{u} + \nabla \mathbf{u}^T)) + \nabla p = \mathbf{F}_g \tag{6}$$

where $\mathbf{u}$ is the local velocity; whereas $\rho$ and $\eta$ are the density and the viscosity of the particles. The material was considered to be Newtonian. Finally, $F_g$ is the gravitational force which was neglected, according to the Eotvos number (Eq. 2).

An ALE approach has been used, where the domain meshes move according to the boundary conditions of the liquid-air interface. The sintering is driven by the surface tension force, which acts normally on the liquid-air interface between the particles and the environment. This was implemented following the approach used by Carin *et al.* [19], where on the open boundary the surface tension $\gamma$ is applied on the curvature $C$ of the two particles (Eq. 7). On the free surface, the meshes move accordingly to the normal velocity $v_n = u_r n_r + u_z n_z$; whereas the meshes displacement on the z and r axes is zero respectively in the r and z directions.

$$[-p\mathbf{I} + \eta(\nabla \mathbf{u} + \nabla \mathbf{u}^T)]\mathbf{n} = C\gamma\mathbf{n} \tag{7}$$

The surface tension was assumed to be constant.

The moisture transfer into the maltodextrin particles was modelled considering Fick Law (Eq. 8) where $C_{H_2O}$ is the amount of water into the particles, and $D_{H_2O-MD}$ is the moisture diffusion coefficient.

$$\frac{\partial C_{H_2O}}{\partial t} + \nabla \cdot ( - D_{H_2O-MD} \nabla C_{H_2O}) = 0 \tag{8}$$

The moisture diffusion coefficient of maltodextrin decreases when the amount of water is increased as reported by Dupas *et al.* [17]. A constant $D_{H_2O-MD}$ was considered in this study, but different simulations considering different $D_{H_2O-MD}$ were performed to ascertain its impact.

At the initial time $t = 0$ the concentration of water into the particles is equal to the concentration at the equilibrium at $RH_0$.

$$t = 0 \quad @ \quad C_{0,H_20} = C_{eq,BET} \tag{9}$$

The moisture transfers through the particle surface depending on the mass transfer coefficient $K$ until the maximum value of concentration in bulk is reached $C_{b,H_2O}$.

$$\text{-}\mathbf{n} \cdot \mathbf{N}_{H_2O} = K(C_{b,H_2O} - C_{H_2O}) \tag{10}$$

The initial and final water concentrations respectively $C_{0,H_2O}$ and $C_{b,H_2O}$ have been chosen according to values of water content corresponding to the relative humidity at the equilibrium respectively $RH_0$ and $RH_b$, at room temperature (T = 25 $°C$).

Maltodextrin 21 particles at the equilibrium were modelled with a Brunauer, Emmett and Teller (BET) sorption isotherm.

$$w_{db} = \frac{M_0 C_{BET} a_w}{(1 - a_w)(1 + (C_{BET} - 1)a_w)} \tag{11}$$

where $M_0$ and $C_{BET}$ are the BET constants and $w_{db}$ is the water content in dry basis.

The moisture absorbed by maltodextrin particles acts as a plasticizer

and when the water content increases the glass transition of the water-maltodextrin mixture $T_{g,mix}$ drops, following a Gordon-Taylor equation:

$$T_g = \frac{k w_{H_2O,wb} T_{g,H_2O} + w_s T_{g,s}}{k w_{H_2O,wb} + w_s} \tag{12}$$

where $k$ is a model constant, $w_s$ and $w_{H_2O}$ are the mass fraction of maltodextrin and water in wet basis; while $T_{g,s}$ and $T_{g,H_2O}$ are respectively the glass transition temperatures of pure water ($T_{g,H_2O} = -135°C$ [9]) and completely dry maltodextrin.

The viscosity of MD DE-21 varies with the room temperature and the $T_{g,mix}$ following a Williams-Landel-Ferry (WLF) model.

$$Log_{10}\frac{\eta}{\eta_g} = \frac{-C_1(T - T_g)}{C_{2,M} + (T - T_g)} \tag{13}$$

where $C_1$ and $C_{2,M}$ are WLF model constants; whereas $\eta_g$ and $T$ are the reference viscosity and temperature. Finally, as suggested by Ubbink *et al.* [4], the constant $C_{2,M}$ for food amorphous polymers depends on the water content and follows a Gordon-Taylor like functions as:

$$C_{2,M} = \frac{k_m w_{H_2O,wb} C_{2,w} + w_s C_{2,s}}{k_m w_{H_2O,wb} + w_s} \tag{14}$$

where $k_m$, $C_{2,w}$ and $C_{2,s}$ are the model constants.

The simulations were carried out using Comsol Multiphysics (V 5.0) using extrafine mesh (with mesh elements having an area of $3.56 \cdot 10^{-2} mm^2$). The effect of the mesh size is discussed in Appendix A. The material properties of Maltodextrin DE-21 and model parameters considered during the simulation, are summarized in table A.1.

Finally, initial bridge ($x_0$), particle size ($d_0$), moisture diffusion coefficient ($D_{H_2O-MD}$), initial and final RH were varied systematically. In table A.2 are reported the values of the considered parameters. Values of $D_{H_2O-MD}$ were chosen in range between $10^{-11}$ and $10^{-13}[m^2/s]$ corresponding respectively to porous and non-porous particles [18].

## 3. Results and Discussion

Firstly, we will discuss how the glass transition temperature and viscosity of maltodextrin vary depending on the water content. Following, a comparison between the sintering model and results shown in the literature is reported. Finally, we study the effect of the moisture transfer on the viscosity and the resulting variation on the sintering kinetics, depending on the particle size, moisture diffusion coefficient, initial and final RH.

### *3.1. Maltodextrin Physical Properties*

The sorption isotherm is shown on the right side of figure A.2 (a); when $a_w$ is low, maltodextrin absorbs a very low amount of water; whereas increasing the relative humidity, the water content increases in a non linear fashion.

Water migrates into the maltodextrin matrix and acts as a plasticizer. The effect of water content on MD 21 $T_{g,mix}$ and viscosity is reported in figures A.2 (a), (b). The increase of water fraction causes a drop of the glass transition temperature of the maltodextrin-water system. The viscosity drastically drops when the $T_{g,mix}$ drops, inducing the flow of material.

### *3.2. Sintering of Homogeneous Particles (No Moisture Sorption)*

In order to compare the sintering model with results reported in the literature a case with homogeneous particles was solved, considering equations 6 and 7 with a constant viscosity.

In figure A.3 a comparison between models is presented. The bridge size and the time were normalized. In particular, the bridge was normalized dividing by the initial diameter as $x/d_0$; whereas the time was is expressed as $t^\star = \frac{2 \cdot t\gamma}{d_0 \eta}$.

The bridge gradually grows from $x_0/d_0$ until a final value of $x/d_0 = 1.26$ is reached, respecting the volume conservation. At earlier times, the sintering kinetics is faster and gradually increases, until the normalized bridge converges to constant value of 1.26. This is proportional to the value of the final diameter for the sintering of two spherical particles $d_f$.

The dimensionless time is inversely proportional to the initial diameter of the particles and the material viscosity, meaning that sintering time increases when the particle size and viscosity are higher; whereas higher surface tension enhances the sintering kinetics.

The model predictions are in good agreement with numerical results. On the other hand, Frenkel-Eshelby and Pokluda models seem to overpredict the bridge size kinetic, at the early stages. Since the Frenkel-Eshelby model assumes a constant radius $R_0$, it diverges to values higher than 1.26 and is not able to predict bridge growth at later stages. In the proposed model, the initial bridge $x_0$ is already defined in order to avoid singularity, therefore it is assumed that at $t = 0s$ particles are already placed in contact.

Figure A.4 shows a comparison between FEM and analytical models.

An initial particle diameter of $d_0 = 1500\mu m$ was considered to enhance the water and viscosity gradients. Each model was solved considering a constant initial and final viscosity, computed respectively at $RH_0$, $RH_b$ and with the coupling. The analytical models were computed solving a Pokluda model considering and an average effective viscosity that follows a WLF model. A similar approach was used by Hartmann & Palzer [1] who considered the model by Rumpf coupled to a WLF effective viscosity.

At long enough timescales, all plots converge to final constant value of $x/d_0 = 1.26$. Moreover, models with a constant $\eta_0$ shows a significantly slower sintering dynamics due to the higher viscosity. On the other hand, both simulations and analytical models with water transfer have an intermediate behaviour between results obtained at constant initial and final viscosity. In fact, at early stages, the high viscosity of maltodextrin slows down the sintering dynamics; whereas, when the water is absorbed into the particles the viscosity significantly drop leading to a more rapid flows and faster bridge growths.

In figure A.4 is shown that FEM simulations result in an initial slower dynamics when compared to the simplified analytical models; whereas, at longer times numerical simulations show faster kinetics. The initial slower dynamics of analytical models can be due to the overestimation of the force acting on the contact area between the two particles at early stages [12].

### *3.3. Velocity Field*

In figure A.5 it is shown the velocity field of the radial cross section of two particles while they sinter and absorb water. The colorbar shows the velocity magnitude; whereas white streamlines indicates the direction of the

flow.

At early stages, the maltodextrin viscosity is higher leading to a lower velocity. After the water diffuses into the particles the drop in viscosity leads to higher velocity, enhancing the bridge growth. This can be observed from the maximum value of the velocity in the colorbars, when the time increases. There is motion of material between the top and the bottom of the particles towards the bridge edges; where it is possible to see a region with higher velocity. On the other hand, in the center of the bridge there is a stagnant region where the material does not flow. Finally, as observed in figure A.8 (f), at t = 150000 s approx. 60% of the overall sintering occurred.

### *3.4. Water and Viscosity Gradients during sintering*

Figure A.7 shows the water and viscosity gradients for two 300 $\mu m$ maltodextrin particles during sintering. At $t = 0s$ the two particles are placed in contact and have a water concentration which corresponds to the water absorbed at the equilibrium at $RH_0$. Afterwards, the moisture diffuses into the particles, leading to lower local viscosity which enhanced the sintering process. At t = 6500 s it is possible to see that even small differences in the water concentrations lead to high viscosity gradients. In fact, the viscosity in the center of the particles is approximately 350% higher compared to their surfaces. Between 19500 and 35000 s, the amount of moisture into the particles keeps increasing, leading to a drop in viscosity in the whole volume. Finally, at 91200 s the water concentration is uniform in both particles; reaching the new equilibrium at $RH_b$ which corresponding to $C_{H2O} = 9.6 mol/m^3$. From this point, the two particles keep sintering together at a constant final viscosity until they minimize their surface area and surface energy.

The water concentration and viscosity were tracked at four different locations of the particles while they sinter. In particular, on the top and the right surfaces, in the center of one particle and in the center of the bridge. A simple sketch which shows the specific locations where the water concentration and viscosity were measured is shown in figure A.6 (a).

Figure A.6 (a), shows a comparison between the local concentration, during sintering of particles of 300 $\mu m$ when the Rh varies from 70 % to 75 %. The concentration on the particle surfaces reaches the equilibrium instantaneously. In the center of the bridge $C_{H2O}$ increases quickly in approximately 0.28 h (1000 s). Afterwards it slightly increases until it reaches the equilibrium in 1.16 days (91200s s). In fact, even though the neck size is very small, in the center of the neck between two particles, there is a stagnant region where the material does not flow, this can explain why the mass transfer is slower. Finally, in the center of the particle the mass transfer is delayed, due to the resistance of diffusion and it reaches the equilibrium in 1.16 days.

The differences in viscosity are reported in figure A.6 (b), showing that during the first 1.16 days there is a difference in viscosity of two order of magnitude between the center of the particle and the surface.

### *3.5. Effect of the Initial Particle Size*

Figure A.8 shows a comparison between the sintering and mass transfer kinetics of particles with different initial size: 100, 200 and 300 $\mu m$; while the RH has been increased from 70 to 75%. On the left side of the graph the normalized bridge is shown; whereas the right side shows the average water concentration inside the maltodextrin particles.

The water concentration rises from approximately 8.5 to 9.75 $mol/m^3$,

making the average viscosity decrease by almost two orders of magnitude from $10^{10}$ to $10^{8} Pa \cdot s$. Particles with higher diameter result in a slower moisture transfer dynamic. In particular, when the particle diameters increases from 100 to 300 $\mu m$, the time at which the water reaches the equilibrium increases approximately five times from 33.3 min (2000 s) to 2.7 h (9700 s). On the other hand, when the maltodextrin particles have a higher diameter, the sintering kinetics is slowed down for the combined effects of the higher particle diameters and the slower drop of the local viscosity.

In table A.3 are reported the characteristic sintering times measured at different RH conditions. $t_{10}$ and $t_{50}$ are respectively the time needed for the material to achieve 10 and 50 % of the overall sintering; whereas $x/d_0(t_{end})$ is the value of the normalized bridge measured at the end of the simulations. The values of $t_{10}$ and $t_{50}$ increases when the particle size is increased, meaning that higher particle size slows down the sintering dynamics. In particular, when the particle size trebles from 100 $\mu m$ to 300 $\mu m$, the 50% of the overall sintering ($t_{50}(x/d_0) = 1.26 \cdot 50\%$) increases from approx. 10h to 31h; whereas the $t_{10}$ increases from 1.5h to 5.3h.

### *3.6. Effect of the Moisture Diffusion Coefficient*

Numerical simulations were solved considering three values of the moisture diffusion coefficient.

As shown in figure A.9 higher moisture diffusion coefficients accelerate the water transfer. In fact, as shown in table A.3, when $D_{H_2O-MD}$ is increased from $10^{-13} m^2/s$ to $10^{-11} m^2/s$ the time needed to reach a new concentration equilibrium into the particles decreases from approx. 3.3 h to 50 min. This has the effect of slowing down the sintering dynamic when $D_{H_2O-MD}$ is equal

to $10^{-13} m^2/s$. On the other hand, the higher moisture diffusion coefficient leads to smaller values of the $N_{m,s}$ that decreases of two order of magnitude, indicating that the mass transfer is very quick compared to the sintering. In this case, the coupling between sintering and mass transfer can be neglected and a simpler simulation considering a constant viscosity corresponding to $\eta_{end}$ can be used to predict the sintering dynamic.

### *3.7. Effect of the Bulk and Initial Relative Humidity*

The water content directly impacts on the local viscosity and finally on the sintering kinetic. Initial and final RH were varied systematically to investigate their effect on the bridge growth.

Figure A.10 shows a comparison between the sintering of two particles of 100 $\mu m$ having the same initial water content of 65% but a different final $RH_b$ respectively 70% and 75%. Increasing the $RH_b$ increases the final concentration of water at the equilibrium from 8.50 to 9.75 $mol/m^3$. Water reaches the equilibrium on approximately 16.6 min (1000 s); however since the final viscosity drops exponentially when the water fraction increases, there is a high variation in the sintering kinetics. As shown in table A.3, the time needed to reach 10% of the overall sintering ($t_{10}(x/d_0) = 1.26 \cdot 10\%$) decreases from approximately 1.73 day to 1.72h.

A comparison between particles of 100 $\mu m$ with different initial RH is reported in figure A.13. When $RH_0$ increases from 65% to 70% the initial concentration into the particles increase from approximately 7.5 to 9.75 $mol/m^3$. However, since the equilibrium is reached very quickly the $RH_0$ does not affect significantly the sintering dynamic.

## 4. Conclusions

In this article, we have presented a computational model to investigate the sintering between two particles of maltodextrin. The model couples the moisture sorption and diffusion process with the bridge growth considering the strong dependency of the viscosity on the water content and the gradients of moisture and viscosity within the particles. The vapour condensation and dissolution timescales were considered slow compared to the other phenomena.

The model predictions are in good agreement with numerical results presented in the literature for homogeneous sintering of two spherical particles and allows predicting the full coalescence of two spherical particles.

Numerical simulations show different dynamics compared to the simplified analytical models because it considers more accurately the role of the force acting on the contact area between the particles. For small enough particles, the intraparticle gradients do not condition significantly the sintering dynamics, as can be anticipated analyzing the characteristic sintering and moisture transfer timescales.

Results show that increasing particle diameter and decreasing the moisture diffusion coefficient slows down moisture transfer to a larger extent than sintering. As a result, when considering a 1.5 mm particle diameter and $D_{H_2O-MD} = 10^{-13} m^2/s$, intraparticle gradients of moisture and viscosity condition significantly the sintering dynamics. A higher final RH drastically enhances the sintering process, due to the higher water fraction into the particles, resulting in a lower final viscosity. On the contrary, a higher initial RH increases the initial water concentration leading to a lower initial viscosity of

maltodextrin; however, the sintering kinetic was not significantly affected.

Maltodextrin DE 21 was used as model material for the model development; however the modelling approach can be used to describe the sintering behaviour all type of amorphous particles. Experimental data should be used as far as available for model validation. Future studies should consider the effect of compaction forces on caking and the effect of a gradual RH change on the moisture transfer and sintering dynamics.

## 5. Acknowledgments

Funding from Nestle' Research is acknowledged.

## Appendix A. Additional Results

### *Appendix A.1. Effect of the Initial Bridge Size*

An initial bridge ($x_0$) is used at time $t = 0s$. A comparison between geometries with different initial bridge is reported in figure A.11. The sintering dynamics can be affected by the dimension of the initial bridge. In particular, if $x_0/d_0$ is higher than 0.016, the sintering dynamic results slightly overestimated due to the higher value of $x_0$. On the other hand, the average concentration plots collapse all on the same curve, therefore the mass transfer is not affected.

### *Appendix A.2. Effect of the Mesh Size and Mesh Quality*

The effect of the initial mesh size on the sintering dynamics is reported in figure A.12 for particles having a $d_0 = 300\mu m$ without water transfer. Moreover, the domain is remeshed automatically when a minimum mesh

quality parameter is reached. Two values were chosen respectively "High Mesh Quality" = 0.2 and "Low Mesh Quality" = 0.01.

Coarser meshes lead to lower faster sintering dynamics. On the other hand, lower mesh quality has the effect of delay the time at which the domain is remeshed.

*Appendix A.3. Effect of the Initial Relative Humidity*

The comparison between particles of 100 $\mu m$ with different initial RH is reported in figure A.13.

## References


[1] M. Hartmann & St. Palzer (2011). *Caking of amorphous powders: material aspects, modelling and applications.* Powder Technology,206 (12):112-121.

[2] U. Zafar, V. Vivacqua, G. Calvert, M. Ghadiri, J.A.S. Cleaver (2017) *A review of bulk powder caking.* Powder Technology 313 (2017) 389–401.

[3] A. Farahnaky, N. Mansoori, M. Majzoobi, F. Badii (2016) *Physicochemical and sorption isotherm properties of date syrup powder: Antiplasticizing effect of maltodextrin* Food and Bioproducts Processing Volume 98, April 2016, Pages 133-141.

[4] J. Ubbink, M. Dupas-Langlet (2020) *Rheology of carbohydrate blends close to the glass transition: Temperature and water content dependence of the viscosity in relation to fragility and strength.* Food Research International 138 (2020) 109801.

[5] Frenkel, J. (1945) *Viscous Flow of Crystalline Bodies under the Action of Surface Tension,* J. Phys., 9, 385 (1945).

[6] O. Pokluda, C. T. Bellehumeur and J. Vlachopoulos (1997) *Modification of Frenkel's Model for Sintering.* AIChE Journal December 1997 Vol. 43, No. 12 , pp 3253- 3256.

[7] R. W. Hopper (1984) *Coalescence of Two Equal Cylinders: Exact Results for Creeping Viscous Plane Flow Driven by Capillarity* Journal of the American Ceramic Society 67(12): C-262-C-264.

[8] C. T. Bellehumeur, M. K. Bisaria, and J. Vlachopoulos *An Experimental Study to Model Assessment of Polymer Sintering.* Polymer Engineering and Science, 1996, Vol. 36, No. 17.

[9] N. Descamps, S. Palzer, Y. H. Roos , J. J. Fitzpatrick (2013) *Glass transition and flowability/caking behaviour of maltodextrin DE 21.* Journal of Food Engineering 119 (2013) 809 - 813.

[10] A. Jagota and P. R. Dawson *Micromechanical Modeling of Powder Compacts-I. Unit Problems for Sintering and Traction Induced Deformation.* Acta meatall. Vol. 36, No. 9, pp. 2551-2561, 1988.

[11] A. Jagota and P. R. Dawson *Simulation of the Viscous Sintering of Two Particles.* J. Am. Ceram Soc 73 111 173-77 (1990).

[12] F. Wakai, K. Katsura, S. Kanchika, Y. Shinoda, T. Akatsu, K. Shinagawa (2016) *Sintering force behind the viscous sintering of two particles.* Acta Materialia 109 (2016) 292 - 299.

[13] G. A. L. van de Vorst *Numerical Simulation of Axisymmetric Viscous Sintering* Engineering Analysis with Boundary Elements 14 (1994) 193-207.

[14] M. A. Walkley,P. H. Gaskell, P. K. Jimack,1 M. A. Kelmanson, and J. L. Summers *Finite Element Simulation of Three-Dimensional Free-Surface Flow Problems.* Journal of Scientific Computing, Vol. 24, No. 2, August 2005.

[15] S. Mukhopadhyay, G. Nimbalkar *Fundamental study on chaotic transition of two-phase flow regime and free surface instability in gas deaeration process.* Experimental and Computational Multiphase Flow, Vol. 3, No. 4, 2021, 258-288.

[16] M. Kamyabi, R. Sotudeh-Gharebagh, R. Zarghami and K. Saleh *Analysis of Non-Isothermal Viscous Flow Coalescence at Micro Scale.* Can. J. Chem. Eng. 97:2565–2572, 2019.

[17] J. Dupas, E. Verneuil, M.Van Landeghem, B. Bresson, L. Forny, M. Ramaioli, F. Lequeux, Talini (2014) *Glass transition accelerates the spreading of polar solvents on a soluble polymer.* PhysRevLett.112.188302 2014-05-09.

[18] *Personal communication of data collected by Nestle' Research Center,* (2020).

[19] M. Carin *Square drop oscillation under surface tension - 2D axisymmetric model.* LIMATB - Universite de Bretagne-Sud.

[20] Verein Deutscher Ingenieure, VDI-Gesellschaft Verfahrenstechnik und Chemieingenieurwesen (GVC), (2010) *VDI Heat Atlas Second Edition* Springer-Verlag Berlin Heidelberg.

[21] N. Descamps, S. Palzer (2007) *Modeling the sintering of water soluble amorphous particles.* AIChE Annual Meeting, Conference Proceedings, January 2007.

[22] J. M. Frias, J. C. Oliveira, K. Schittkowski (2007) *Modeling and Parameter Identification of a Maltodextrin DE 12 Drying Process in a Convection oven* AIChE Annual Meeting, Conference Proceedings, January 2007.

[23] F. A. Mohos (2010) *Confectionery and Chocolate Engineering: Principles and Applications: Appendix 1 -Data on engineering properties of materials used and made by the confectionery industry.*

[24] N. Castro, V. Durrieu, C. Raynaud, A. Rouilly (2016) *Influence of DE-value on the physicochemical properties of maltodextrin for melt extrusion processes.* Carbohydrate Polymers 144 (2016) 464–473.

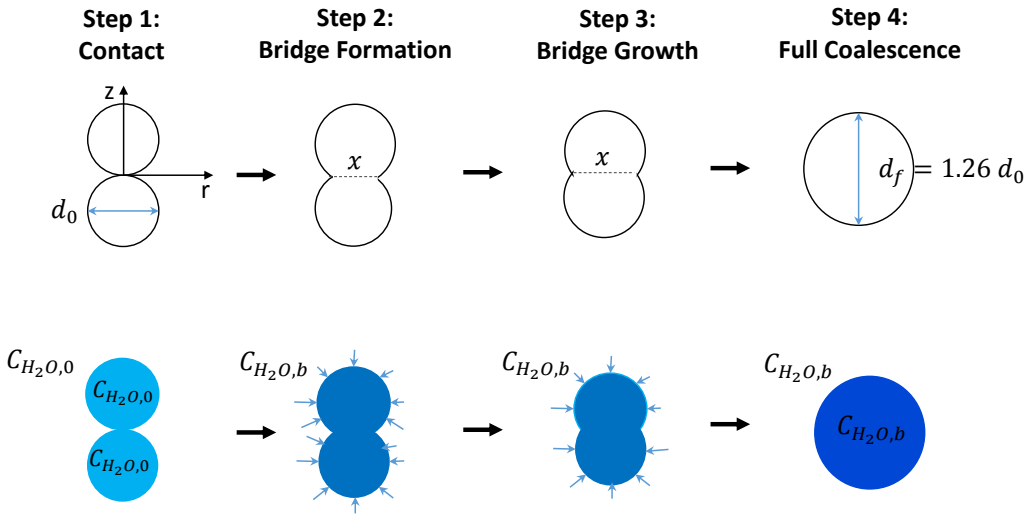


Figure A.1: *Schematic representation of sintering between two particles while the absorb moisture from the environment due to a RH increase.*

Table A.1: Maltodextrin DE-21 Model Parameters.

| Parameter | Value | Unit | Ref. |
|---|---|---|---|
| $\rho$ | 1405 | $[kg/m^3]$ | [22] |
| $\gamma$ | $60 \cdot 10^{-3}$ | $[N/m]$ | [1] [21] |
| $K$ | 0.146 | $[m/s]$ | [-] |
| $M_0$ | 0.045 | $[-]$ | [18] |
| $C_{BET}$ | 25.5 | $[-]$ | [18] |
| $k_{GT}$ | 7.31 | $[-]$ | [18] |
| $T_{g,s}$ | 152.9 | $[^\circ C]$ | [18] |
| $T_{g,H2O}$ | -135 | $[^\circ C]$ | [18] |
| $T$ | 25 | $[^\circ C]$ | [-] |
| $\eta_g$ | $10^{12}$ | $[Pa \cdot s]$ | [18] |
| $C1_{WLF}$ | 17.4 | $[-]$ | [4] |
| $k_m$ | 0.81 | $[-]$ | [4] |
| $C_{2,c}$ | 59.0 | $[^\circ C]$ | [4] |
| $C_{2,w}$ | 19.5 | $[^\circ C]$ | [4] |

Table A.2: MD 21 parameters varied during the parametric study.

| Parameter | Value | Unit |
|---|---|---|
| $x_0/d_0$ | [0.01, 0.016, 0.033] | [-] |
| $d_0$ | [100, 200, 300, 1500] | $[\mu m]$ |
| $D_{H_2O-MD}$ | [$10^{-11}$, $10^{-12}$, $10^{-13}$] | $[m^2/s]$ |
| $RH_0$ | [60, 65, 75] | [%] |
| $RH_b$ | [70, 75] | [%] |

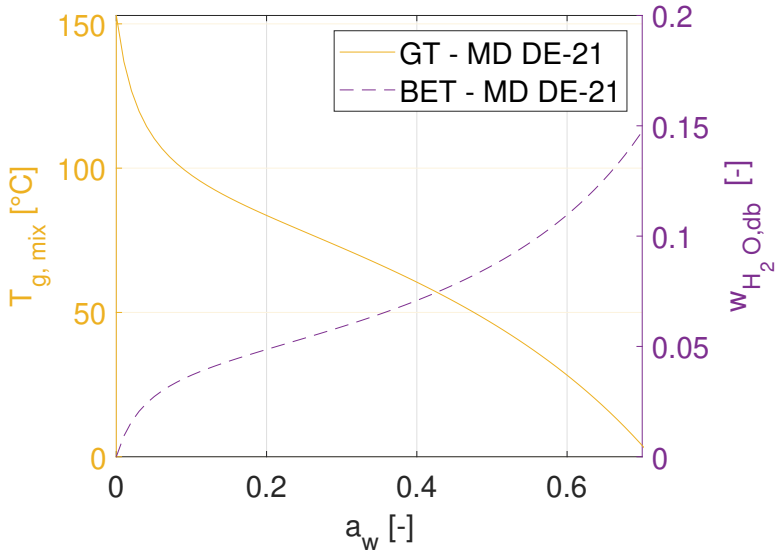


(a) *MD 21 Sorption Isotherm (dotted purple line) and Glass Transition Temperature vs water content (continuous gold line).*

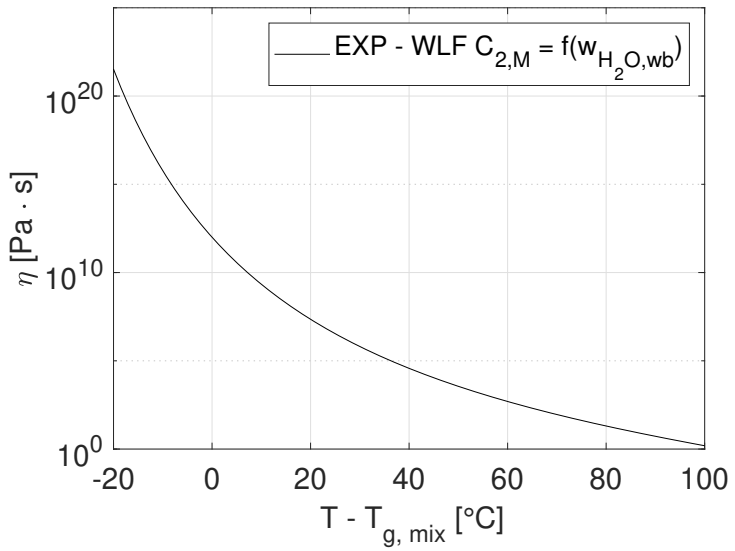


(b) *MD 21 Viscosity ($\eta$)*

Figure A.2: *Effect of Water content on MD 21 Physical properties.*

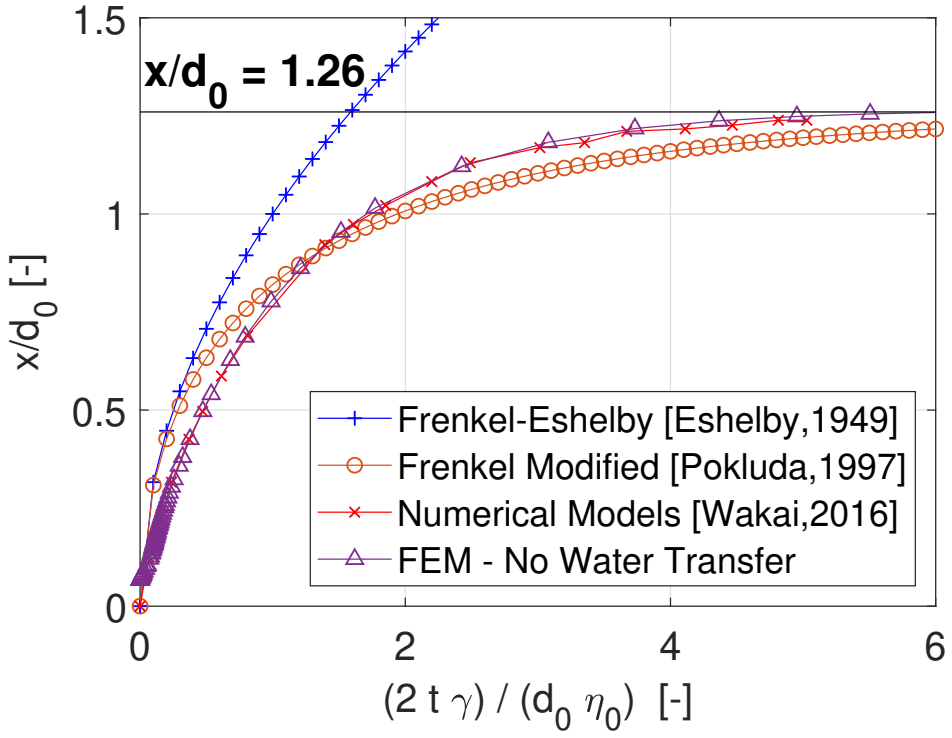


Figure A.3: Comparison between the homogeneous sintering (purple triangle) model proposed in this study, solved with an ALE method, and different models reported in the literature respectively: Frenkel-Eshelby Model (blue plus), Pokluda Model (orange circle) and Numerical Models from Wakai et al. (red cross).

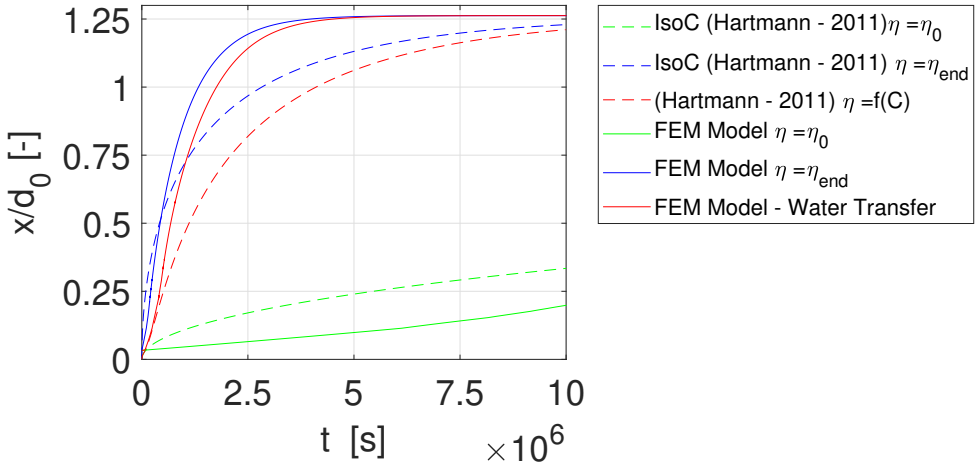


Figure A.4: Comparison between FEM (continuous lines) and analytical (dotted lines) solved at respectively: $\eta = \eta_0$ (green), $\eta = \eta_{end}$ (blue) and $\eta = f(C)$ (red). Models with moisture transfer were solved considering $d_0 = 1500\mu m$, $RH_0 = 70\%$, $RH_b = 75\%$ and $D_{H_2O-MD} = 10^{-13} m^2/s$.

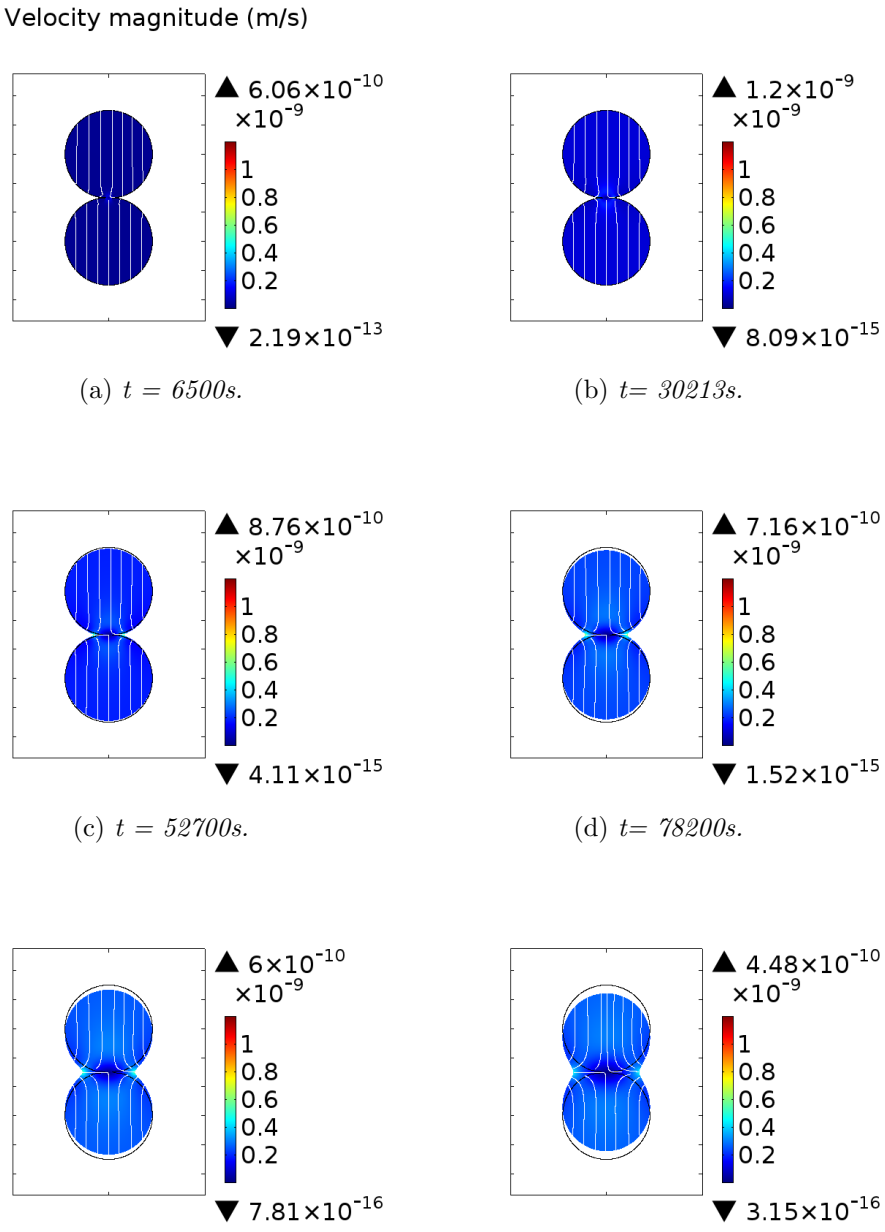


(a) $t$ = *6500s.*

(b) $t$= *30213s.*

(c) $t$ = *52700s.*

(d) $t$= *78200s.*

(e) $t$ = *104100s.*

(f) $t$= *150000s.*

Figure A.5: *Velocity field of two MD DE-21 particles having an initial diameter* $d_0 = 300\mu m$ *sintering while the RH increases from 70 to 75%. The simulation was solved considering* $D_{H_2O-MD} = 10^{-13}m^2/s$. *The upward and downward arrows indicate the maximum and minimum values of the velocity.*

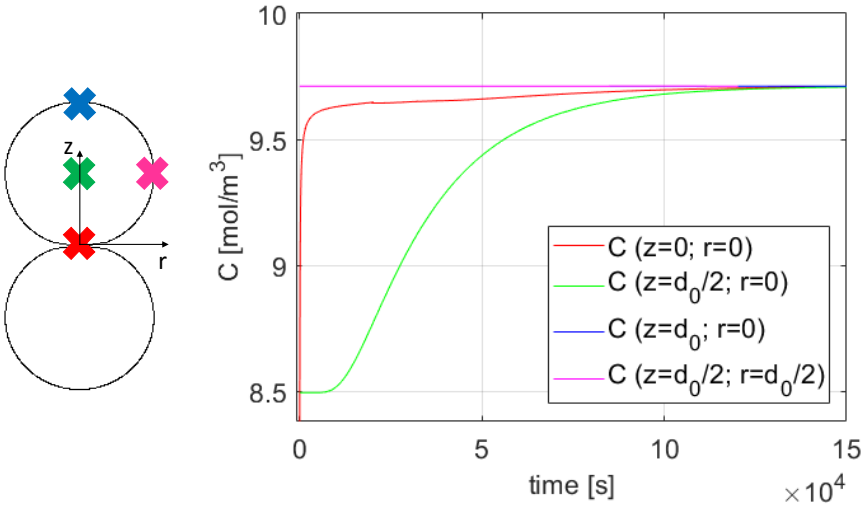


(a) *Moisture concentration measured at different coordinates.*

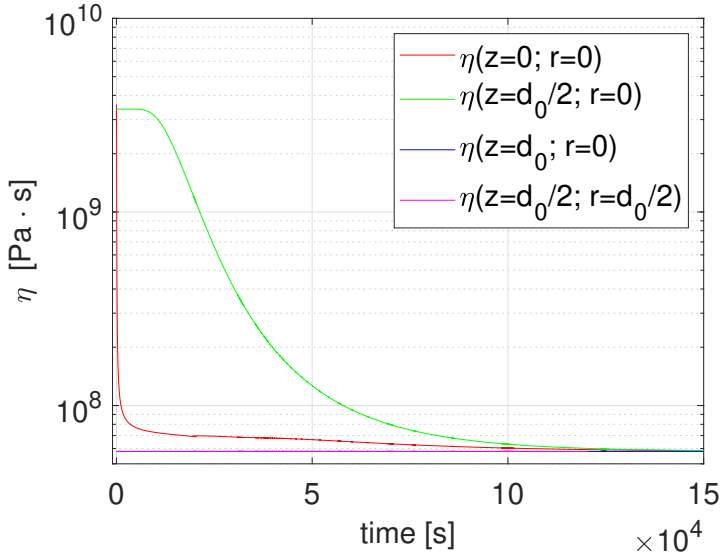


(b) *Viscosity measured at different coordinates.*

Figure A.6: *Moisture concentration and viscosity measured in different location of particles respectively: the center of the bridge (red), the center of one particle (green), the top surface of the particle (blue) and the right surface (magenta). The simulation was carried out assuming* $d_0 = 300\mu m$, $RH_0 = 70\%$, $RH_b = 75\%$ *and* $D_{H_2O-MD} = 10^{-13} m^2/s$. *The blue and magenta lines overlap.*

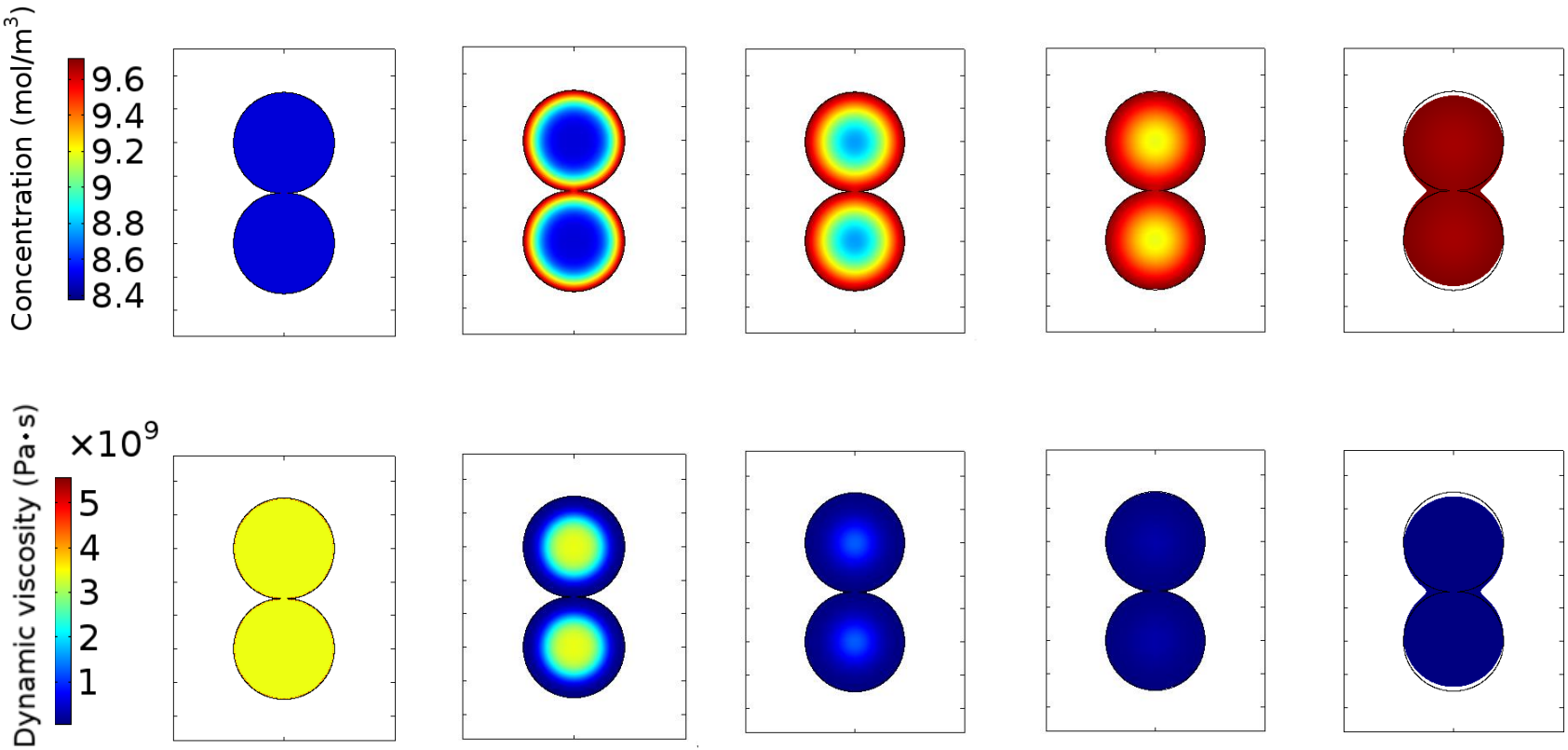


Figure A.7: *Water and viscosity gradients during the sintering of two spherical particles while they absorb water. The simulation was solved assuming* $d_0 = 300\mu m$, $RH_0 = 70\%$, $RH_b = 75\%$ *and* $D_{H_2O-MD} = 10^{-13}m^2/s$.

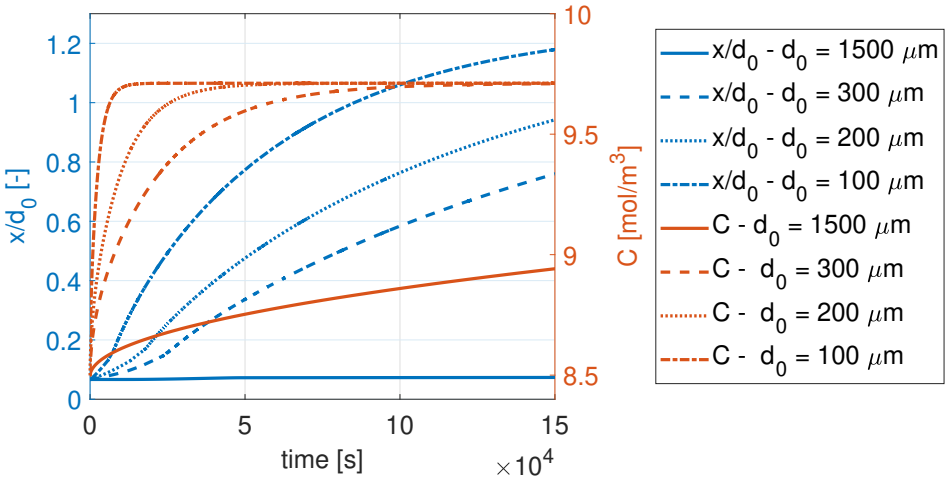


Figure A.8: Comparison of sintering and mass transfer dynamics when the RH has been increased from 70 to 75% in particles with a different initial diameter respectively: $d_0 = 1500\mu m$ (continuous line), $d_0 = 300\mu m$ (dashed line), $d_0 = 200\mu m$ (dotted line) and $d_0 = 100\mu m$ (dot-dashed line). All simulations were solved considering $D_{H_2O-MD} = 10^{-13} m^2/s$.

Table A.3: Characteristic sintering time measured at different conditions. The final time of the simulations is $t_{end} = 15 \cdot 10^4 s$.

| $d_0$ $[\mu m]$ | $RH_0$ [%] | $RH_b$ [%] | $D_{H_2O-MD}$ $[m^2/s]$ | $t_{10}$ $\times 10^4[s]$ | $t_{50}$ $\times 10^4[s]$ | $x/d_0(t_{end})$ $[-]$ |
|---|---|---|---|---|---|---|
| 100 | 65 | 70 | $10^{-13}$ | - | - | 0.10 |
| 100 | 65 | 75 | $10^{-13}$ | 0.62 | 3.67 | 1.19 |
| 100 | 70 | 75 | $10^{-13}$ | 0.54 | 3.62 | 1.19 |
| 200 | 70 | 75 | $10^{-13}$ | 1.21 | 7.41 | 0.94 |
| 300 | 70 | 75 | $10^{-13}$ | 2.79 | 12.1 | 0.73 |
| 1500 | 70 | 75 | $10^{-13}$ | - | - | 0.07 |
| 300 | 70 | 75 | $10^{-11}$ | 2.16 | 11.22 | 0.76 |
| 300 | 70 | 75 | $10^{-12}$ | 2.20 | 11.28 | 0.76 |

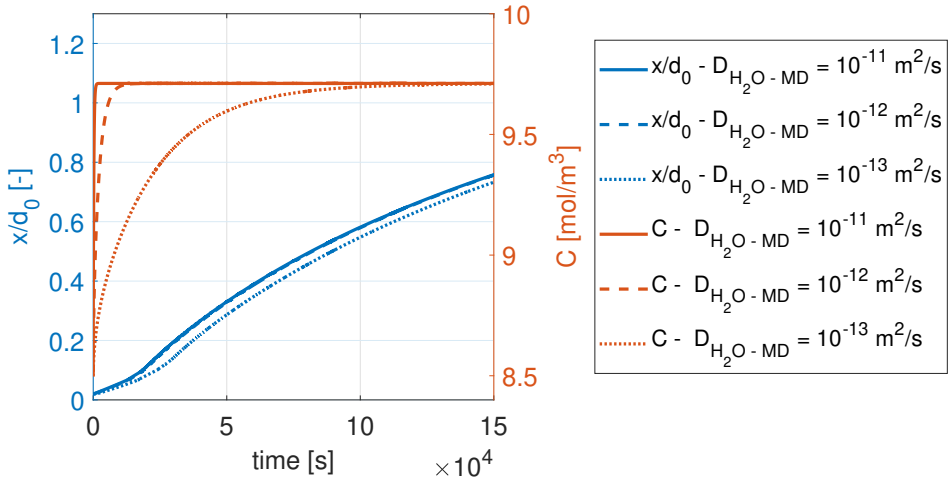


Figure A.9: Comparison of sintering and mass transfer dynamics of particles with $d_0 = 300\mu m$, $RH_0 = 70\%$ and $RH_b = 75\%$ having different moisture diffusion coefficients respectively: $D_{H_2O-MD} = 10^{-11}m^2/s$ (continuous line), $D_{H_2O-MD} = 10^{-12}m^2/s$ (dashed line), $D_{H_2O-MD} = 10^{-13}m^2/s$ (dotted line). In the simulations with $D_{H_2O-MD} = 10^{-11}m^2/s$ and $10^{-12}m^2/s$ the $x/d_0$ plots overlap.

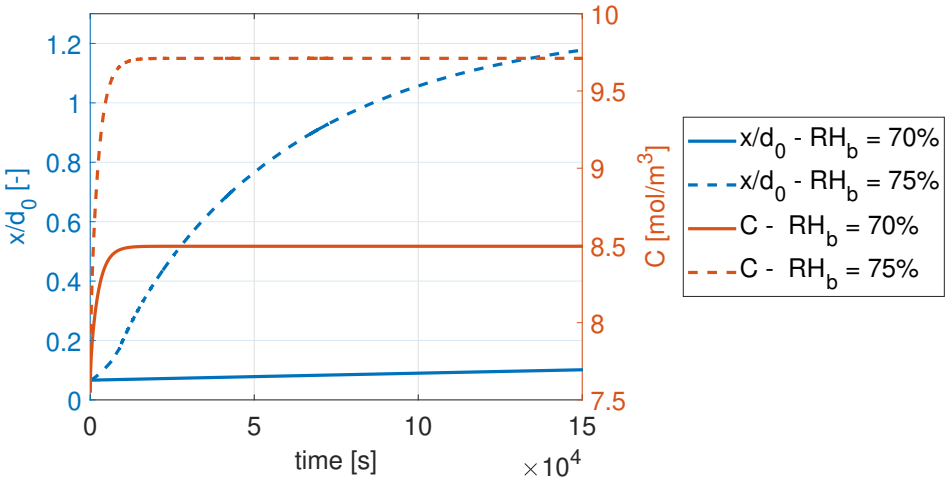


Figure A.10: Comparison between particles with $d_0 = 100\mu m$, $RH_0 = 65\%$ and different final $RH_b$ respectively: $RH_0 = 70\%$ (continuous line), $RH_0 = 75\%$ (dash line). Simulations were solved considering $D_{H_2O-MD} = 10^{-13} m^2/s$.

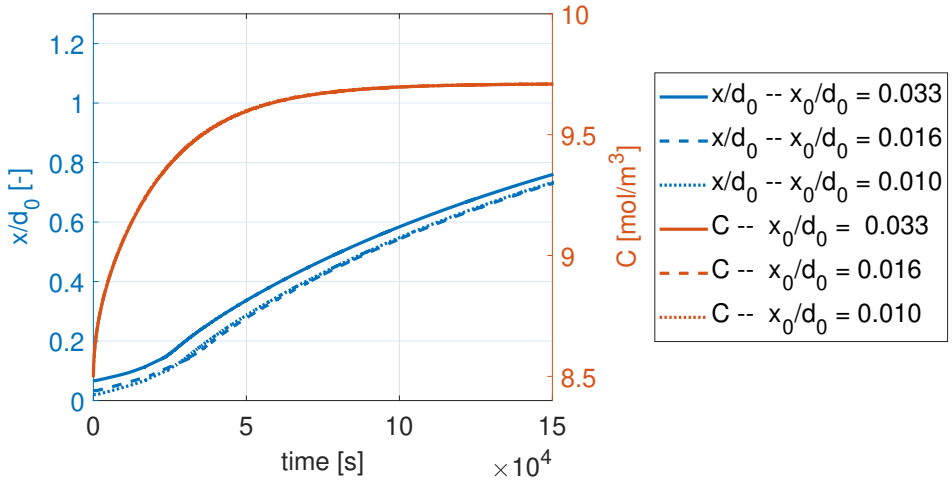


Figure A.11: Comparison between particles with a different initial bridge respectively: $d_0/x_0 = 0.033$ (continuous line), $d_0/x_0 = 0.016$ (dash line) and $d_0/x_0 = 0.010$ (dotted line). Simulations were solved considering $d_0 = 300\mu m$, $RH_0 = 70\%$ and $RH_b = 75\%$. Simulations were solved considering $D_{H_2O-MD} = 10^{-13} m^2/s$.

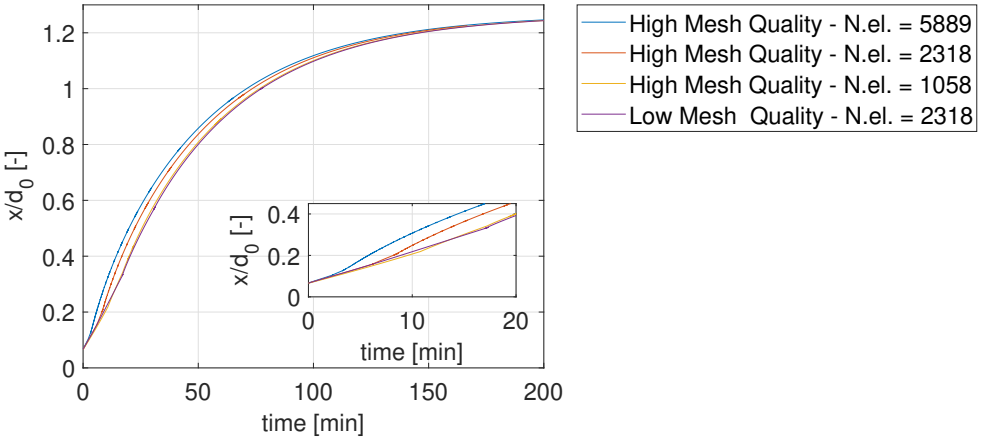


Figure A.12: Comparison of simulations solved with different initial mesh number and mesh quality: 5889 (blue), 2318 (orange), 1058 (yellow), 2318 (purple).

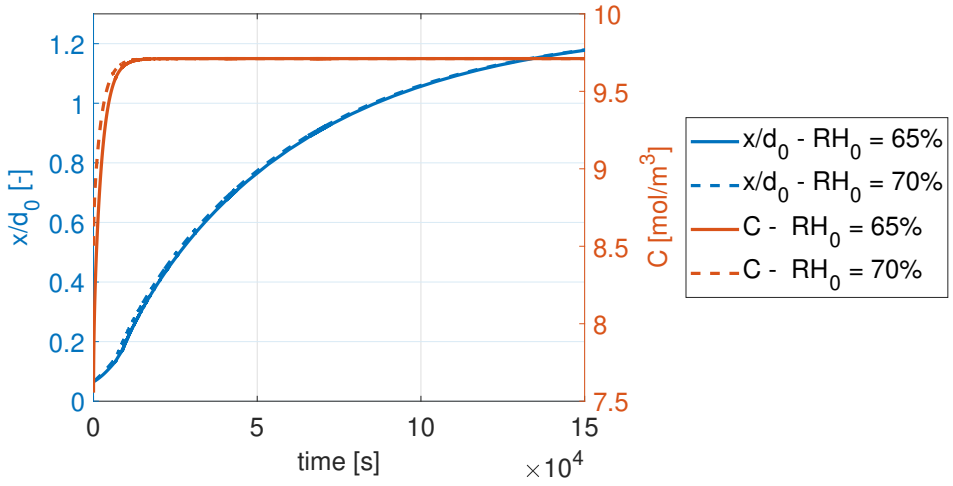


Figure A.13: Comparison between particles with $d_0 = 100\mu m$, $RH_b = 75\%$ and different initial $RH_0$ respectively: $RH_0 = 65\%$ (continuous line), $RH_0 = 70\%$ (dash line).